Shear banding as a cause of nonmonotonic stress relaxation after flow cessation

Vanessa K. Ward [*] and Suzanne M. Fielding
Department of Physics, Durham University, South Road, Durham DH1 3LE, United Kingdom

Recent flow cessation experiments on soft materials have shown a counterintuitive nonmonotonic relaxation of the shear stress: following the switch off of a steady imposed shear flow, the stress initially decays before later increasing again. By simulating the soft glassy rheology model in a form extended to allow steady state shear banding, we show that the presence of shear bands prior to flow cessation can give rise to this phenomenon. We give a mechanistic understanding of the basic physics involved, in terms of (i) the decay of the shear bands after flow cessation, and (ii) the evolution of frustrated local stresses, governed by different time scales for plastic relaxation in each band. In particular, an elastic recoil in the unsheared band gives rise to negative local frustrated stresses, the slow release of which can cause an increase in macroscopic stress. Given that shear banding and frustrated local stresses arise widely across disordered soft solids, we argue that nonmonotonic stress relaxation after flow cessation may occur in many different materials.

Introduction. Soft materials such as colloids, polymers, emulsions, and granular matter display rich rheological behavior, arising from the interaction of their constituent substructures (polymer chains, emulsion droplets, etc.) with an imposed flow [1]. For any such material, a key rheological fingerprint is the "flow curve" relating shear stress and shear rate in steady shear, $\sigma_{ss}(\dot{\gamma})$. For a broad class of amorphous "soft glassy materials," including dense colloids, foams, emulsions, and low density gels, this displays a nonzero yield stress $\sigma_y = \lim_{\dot{\gamma} \to 0} \sigma_{ss}$ [2–4]. When subject to a load $\sigma < \sigma_y$, such materials show an elastic solidlike response, or slow creep, with their constituent substructures unable to rearrange significantly. In contrast, larger loads $\sigma > \sigma_y$ facilitate rearrangements, leading to yielding and the onset of liquidlike flow. Significant effort has been devoted to understanding this solid-to-liquid yielding transition, as reviewed in Ref. [5].

In recent years, attention has increasingly turned to understanding the reverse liquid-to-solid transition that arises on flow cessation. Starting from an initial state of steady shear with stress $\sigma_{ss}(\dot{\gamma})$, the shear rate is switched to zero at some time, defined as $t = 0$, and the subsequent stress decay observed, $\sigma(t > 0)$. Typically, this decay shows a broad spectrum of relaxation timescales, with fast initial decay modes pertaining to the rearrangement of substructures on small length scales, and slower modes signifying larger scale restructuring. In soft glasses, the decay is often nonintegrable [6–12], either with $\sigma \sim t^{-\beta}$ and $0 < \beta < 1$ or asymptoting to a nonzero constant $\sigma_{res} = \lim_{t \to \infty} \sigma(t)$. The residual stress σ_{res} then provides a macroscopic signature of frustrated

stresses that remain trapped locally within the material, as captured in molecular simulations [9], elastoplastic models [9], and mode coupling theory [12]. It plays a significant role in controlling mechanical memory [13–16] and performance [17], as in the spectacular exploding "Rupert's drop" phenomenon [18]. For a review, see [19].

For decades, it has been implicitly assumed that the stress must decay monotonically as a function of time t after flow cessation, whether to zero or a nonzero residual value σ_{res}. However, recent experiments have challenged this assumption: a remarkable nonmonotonic stress decay following flow cessation was reported in boehmite gels [20] and in three different self-associating organo/supramolecular gels [21]. Nonmonotonic stress evolution has also been seen following more complicated two-stage compression protocols in granular matter [22], crumpled sheets [23], and particle simulations [24].

To date, such observations remain poorly understood theoretically. Indeed, it is difficult to intuit a mechanism via which stress can increase over any time interval, once shear driving no longer acts on the material. In associating gels [21], it was suggested to arise via the reformation of broken bonds after flow cessation. The released energy was argued to then increase the system's elastic energy via the formation of domains partly aligned with the prior shear. Within a phenomenological structural kinetic model [25], the stress increase was predicted to arise due to the competition of viscoelastic aging with rejuvenation. In the context of constitutive modeling of thixotropy, the buildup of a material's modulus over time has been argued to violate the second law of thermodynamics [26], although elasticity was argued to contribute significantly to thixotropy in Ref. [27].

In this Letter, we put forward an alternative explanation for the phenomenon of nonmonotonic stress relaxation after flow cessation. In particular, we argue that the widespread physical ingredients of (i) coexisting shear bands of differing viscosity prior to flow cessation and (ii) frustrated local stresses can

---

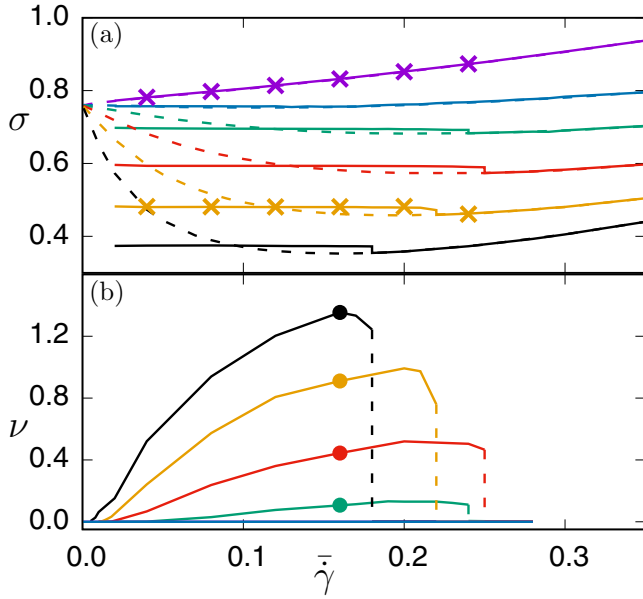*Contact author: vanessa.k.ward@durham.ac.uk

FIG. 1. (a) Steady state flow curves of shear stress as a function of shear rate (solid lines) and constitutive curves for shear artificially constrained to be homogeneous (dashed lines). In curves from top to bottom, the coupling parameter $a = 0.0, 1.0, 2.0, 4.0, 8.0, 16.0$. Crosses indicate shear rates for which the stress decay after flow cessation is explored in Fig. 2. (b) Nonmonotonicity parameter ν, as defined in the main text. The delay time is $\tau_x = 100$ and a increases in curves from bottom to top. Dots indicate the systems explored in Fig. 3.

interact to give rise to it. We substantiate this scenario by simulating the widely used soft glassy rheology model, in a form extended to allow shear banding. It is known that shear banding is present in a number of the systems that exhibit the stress increases [28]. We furthermore offer a detailed mechanistic understanding of the basic underlying physics, which can be understood via the evolving distributions of frustrated local stresses in the two former bands, governed by their differing effective temperatures.

The SGR model considers an ensemble of elastoplastic elements exploring an energy landscape of traps [29,30]. Each element corresponds to a mesoscopic region of material that is large enough to allow the definition of a local continuum shear strain l and shear stress kl, with modulus k the same for all elements. The macroscopic elastoplastic stress is the average of the elemental ones, $\sigma = k\langle l \rangle$. Under an imposed shear of rate $\dot{\gamma}$, each element strains at rate $\dot{l} = \dot{\gamma}$, leading to an elastic buildup of stress. Elemental stresses are also intermittently released via local plastic events, occurring stochastically at rate $r = \tau_0^{-1} \min\{1, \exp[-(E - \frac{1}{2}kl^2)/x]\}$, with a microscopic attempt time τ_0, trap energy depth E, and noise temperature x. After yielding, an element resets its local strain l to zero and hops into a new trap of depth drawn from an exponential distribution $\rho(E) = \exp(-E/x_g)/x_g$. This gives a glass transition at $x = x_g$ [31] and rheological ageing for $x < x_g$ [32].

The SGR model was extended in Ref. [33] to capture a multivalued constitutive curve $\sigma(\dot{\gamma})$ for states of stationary homogeneous shear (dashed lines in Fig. 1). Shear bands can then form when spatial heterogeneity is allowed in the flow-

gradient direction y, giving a flat plateau in the steady state flow curve (solid lines in Fig. 1). The extended model allows the noise temperature $x = x(y, t)$ to evolve according to

$$\tau_x \frac{\partial x}{\partial t} = -x + x_0 + a\langle rl^2 \rangle + \lambda^2 \frac{\partial^2 x}{\partial y^2}. \quad (1)$$

Here x_0 is a bare noise temperature, a the magnitude of a coupling term representing the pumping of noise by jump events, τ_x a delay time for the relaxation of x, and λ a lengthscale that sets the width of the interface between shear bands. To simulate this model in shear, we place M SGR elements on each of S streamlines stacked across the flow gradient direction from $y = 0$ to L_y. For an imposed shear rate $\bar{\dot{\gamma}}(t)$ averaged across streamlines, the local shear rate $\dot{\gamma}(y, t)$ in creeping flow follows by setting the total stress $\Sigma = \sigma(y, t) + \eta\dot{\gamma}(y, t) = \bar{\sigma}(t) + \eta\bar{\dot{\gamma}}(t)$, with η a small solvent viscosity, giving 1D Eshelby stress propagation [34]. Force balance constrains Σ to be uniform across y.

Protocol. We simulate a shear protocol as follows. First, we apply a strong preshear of rate $\bar{\dot{\gamma}}_{\text{pre}}$, for a time sufficient to attain a fully fluidized steady state. Second, we drop the shear rate to some value $\bar{\dot{\gamma}}$ and hold it constant for a duration t_{ss}, sufficient for the stress to attain a steady state prescribed by the flow curve $\sigma_{\text{ss}}(\bar{\dot{\gamma}})$. (To facilitate a more rapid numerical evolution to a banded state, we evolve the system initially with a small τ_x before introducing the τ_x of interest only once the stress has reached a steady state at $t = -500$.) Although the macroscopic stress attains a steady state, the low shear band still slowly ages. The shear is then switched off by setting $\bar{\dot{\gamma}} = 0.0$ at time $t = 0$ and the stress relaxation is tracked as function of time post switch off.

Parameters. The parameters of the model are the modulus k, microscopic time τ_0, glass transition temperature x_g, bare noise temperature x_0, coupling parameter a, delay time τ_x, stress diffusivity λ, and solvent viscosity η. The flow device has gap size L_y. The parameters of the protocol are the rate of preshear $\bar{\dot{\gamma}}_{\text{pre}}$, the duration t_{ss} of shearing at the shear rate of interest prior to switch off, and that shear rate $\bar{\dot{\gamma}}$. Numerical parameters are the number of streamlines S and elements per streamline M, and the timestep dt. We choose units of stress $k = 1$, time $\tau_0 = 1$, and length $L_y = 1$. We also set $x_g = 1.0$, thereby setting the yield strain $O(1)$. Unless otherwise stated we then set $x_0 = 0.3$, $\lambda = 0.01$, $\eta = 0.05$, $\bar{\dot{\gamma}}_{\text{pre}} = 10.0$, $t_{\text{ss}} = 1000.0$, $S = 100$, $M = 1000$, and $dt = 0.001$ (increased to $dt = 0.01$ for $t > 10\,000$.) Important parameters to explore are the coupling parameter a, the imposed shear rate $\bar{\dot{\gamma}}$, and the delay time τ_x. In particular, a controls the effective temperature and therefore, together with $\bar{\dot{\gamma}}$, the extent of shear banding prior to flow cessation. The delay time τ_x controls the relaxation of the effective temperature, and therefore also of the bands, after cessation.

Results. We start in Fig. 1(a) by showing the flow curves of shear stress as a function of shear rate in steady shear prior to switch off, $\sigma_{\text{ss}}(\bar{\dot{\gamma}})$. Solid lines correspond to systems in which the shear field is allowed to become heterogeneous. Dashed lines show the underlying constitutive curves, with the shear artificially constrained to be uniform. For $a > a^* \approx 0.84$, the constitutive curves are nonmonotonic, with a regime of negative slope $d\sigma/d\dot{\gamma} < 0$ that causes shear bands to form over a window of shear rates $0 < \bar{\dot{\gamma}} < \bar{\dot{\gamma}}_c(a)$. Over this window,
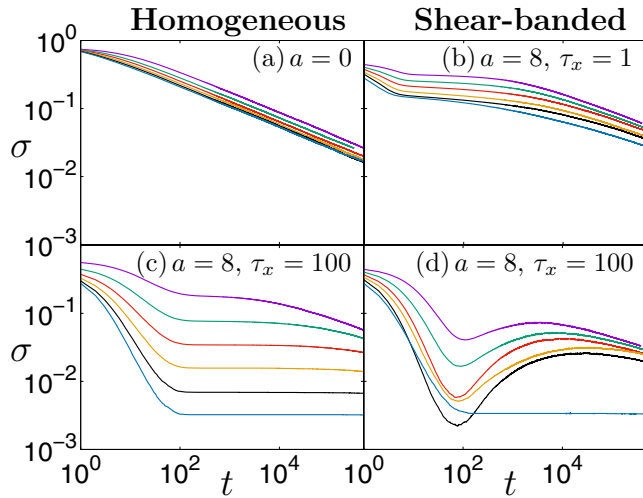
FIG. 2. Relaxation of the shear stress σ as a function of time t after flow cessation. The shear rates prior to switch-off are $\dot{\gamma} = 0.04, 0.08, ..., 0.24$ [indicated by crosses in Fig. 1(a) in curves from top to bottom in each panel]. (a) Coupling parameter $a = 0.0$: homogeneous shear prior to flow cessation. (b) $a = 8.0$ and $\tau_x = 1.0$: shear-banded but x decays quickly. (c) $a = 8.0$ and $\tau_x = 100.0$: homogeneous shear (artificially constrained.) (d) $a = 8.0$ and $\tau_x = 100.0$: shear-banded (except at the largest $\bar{\gamma} = 0.24$) and x decays slowly.

FIG. 3. Nonmonotonicity parameter $\nu = \log_{10}(\sigma_{\max}/\sigma_{\min})$ for $\bar{\gamma} = 0.16$. (a) Plotted vs delay time τ_x for $a = 1.0, 2.0, 4.0, 8.0, 16.0$ in curves from bottom to top. ($\nu = 0$ for $a = 1.0$.) (b) Plotted vs coupling parameter a for $\tau_x = 1.0, 10.0, 100.0, 1000.0, 5000.0$ in curves from bottom to top. ($\nu = 0$ for $\tau_x = 1.0$.) The dots show parameter values from Fig. 1(b).

the flow curves are flat and differ from the homogeneous constitutive curve. The strain rates in the two shear bands that form in this regime correspond to the shear rates at each end of the plateau in the steady state flow curve. The proportion of the gap occupied by each band is such that the shear rate averaged over the two bands, across the gap, equals the applied strain rate. The interface between the two bands has a slightly diffuse width governed by the prefactor λ in the final term of Eq. (1). For $\bar{\gamma} > \bar{\gamma}_c$, the shear is again homogeneous, and the constitutive and flow curves coincide. In principle, the flat stress plateau should extend rightwards until it intersects the constitutive curve. In practice, for higher shear rates in this regime the system gets stuck in a state of metastable homogeneous shear, giving a slight step in the flow curve.

Figure 2 shows the relaxation of the shear stress as a function of time t following shear cessation, starting from a state of steady shear prescribed by the flow curves just discussed, such that $\sigma(t = 0^+) = \sigma_{ss}$. Two values of the coupling parameter a are explored. For $a = 0.0$ the underlying constitutive curve in Fig. 1 is monotonic, the shear prior to flow cessation is homogeneous, and the stress decay in Fig. 2(a) is monotonic for all values of shear rate simulated [indicated by purple crosses in Fig. 1(a)].

For $a = 8.0$, in contrast, the underlying constitutive curve is nonmonotonic and the shear prior to flow cessation is banded for most shear rates indicated by yellow crosses in Fig. 1, in any simulation that allows spatial heterogeneity in the flow-gradient direction y. We then find the stress decay after flow cessation to be nonmonotonic, provided the delay time τ_x is sufficiently large; see Fig. 2(d). (An exception is seen for the highest shear rate, where the flow prior to switch off is homogeneous, resulting in monotonic stress decay after switch off). In simulations performed for the same
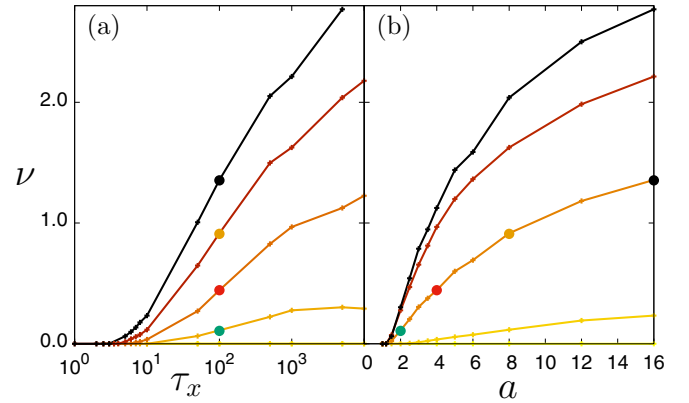
parameter values, but with the shear field artificially constrained to be homogeneous, the stress decay after cessation is always monotonic [Fig. 2(c)]. For the smaller delay time $\tau_x = 1.0$ in Fig. 2(b), the stress decay after cessation is also monotonic, even with banded flow prior to cessation.

Taken together, the results in Fig. 2 suggest that two conditions are needed for nonmonotonic stress relaxation after flow cessation. The first is the presence of shear bands in the steady state prior to flow cessation. The second is a sufficiently large delay time τ_x in the relaxation of the effective temperature after flow cessation—which, as we shall see below, controls the evolution of the local stress distributions post switch off.

To explore further the dependence of this phenomenon on the parameters of the model, we quantify the degree to which the stress decay after flow cessation is nonmonotonic in any simulation via the parameter $\nu = \log_{10}(\sigma_{\max}/\sigma_{\min})$. Here $\sigma_{\min}$ is the local minimum in the stress relaxation, which occurs around a time $O(10^2)$ for the data in Fig. 2(d), and $\sigma_{\max}$ the local maximum, around a time $O(10^4)$. A value $\nu = n$ thus corresponds to a stress rise of n orders of magnitude. The values obtained for ν are averaged over ten simulation runs.

This nonmonotonicity parameter ν is plotted in Fig. 1(b) versus the shear rate prior to flow switch off, for several values of the coupling parameter a and a delay time $\tau_x = 100.0$. For $a < a^*$, the shear prior to flow cessation is homogeneous and the stress decay after flow cessation is monotonic ($\nu = 0.0$) at all shear rates. For $a > a^*$ the shear prior to flow cessation is banded for a range of shear rates $0 < \bar{\gamma} < \bar{\gamma}_c$ and the stress decay after flow cessation can be nonmonotonic, $\nu > 0.0$. In this regime, ν increases with increasing shear rate $\bar{\gamma}$, and hence with the width of the high shear band. The value of ν then reaches a peak before declining slightly then falling precipitously to zero once homogeneous shear is recovered for $\bar{\gamma} \gtrsim \bar{\gamma}_c$.

For one particular imposed shear rate, $\dot{\gamma} = 0.16$, shown by dots in Fig. 1(a), we also explore the effect of varying the delay time τ_x [Fig. 3(a)] and the coupling parameter a [Fig. 3(b)]. As can be seen, to obtain a nonmonotonic stress

decay after flow cessation, $\nu > 0$, a sufficiently large value of the coupling parameter is required, $a \geqslant a^{**} > a^*$. This ensures that the flow state prior to switch off is shear banded, and with a sufficiently large effective temperature difference between the bands. For $a > a^{**} \approx 1.5$, ν then increases with increasing a. Also required is a sufficiently long delay time for the relaxation of the effective temperature post switch off, $\tau_x \geqslant \tau_x^* \approx 5.0$. For $\tau_x > \tau_x^*$, ν then increases with τ_x. The time at which the stress reaches a minimum is largely independent of the imposed shear rate and the coupling parameter a, but increases linearly with the parameter τ_x that governs the timescale for the evolution of the effective temperature in Eq. (1).

Mechanistic understanding. We now explain the physical mechanism of this phenomenon. We do so with reference to the distribution of local strains l, or equivalently of local stresses kl (recall $k = 1$). This is plotted at several times after flow cessation in the region previously (during flow) occupied by the high shear band in Figs. 4(b) and 4(c); and in the region previously occupied by the low shear band in Figs. 4(d) and 4(e). We have checked that the width of these two regions stays relatively constant during the stress relaxation after flow cessation.

Consider a shear banded state before switch off, with averages over elements in the high shear band and unsheared band denoted $\langle\cdot\rangle_h$ and $\langle\cdot\rangle_u$. In the high shear band, the strong shear will have fluidized the material, with elements occupying shallow traps of high average yielding rate $\langle r \rangle_h$. In the unsheared band the material will be solidlike, elements having aged into deep traps with low $\langle r \rangle_u$. Force balance, however, demands a uniform shear stress, $\sigma = \langle l \rangle_h = \langle l \rangle_u$.

Consider now the system's evolution after the shear is switched off. The rate of change of stress $\dot{\sigma} = \langle \dot{l} \rangle_i = \dot{\gamma}_i - \langle lr \rangle_i$, with a rate of elastic stress evolution $\dot{\gamma}$, and of plastic stress relaxation $\langle lr \rangle$. This applies separately in the fluidized and solidlike regions, previously occupied by the high and low shear bands for which we keep the labels $i = $ h, u even after switch off. Indeed, each region has a nonzero shear rate $\dot{\gamma}_{h,u}$ for some time after the shear is switched off, but now with zero average, $\bar{\dot{\gamma}} = 0$.

In the fluidized region, the rate of plastic stress relaxation $\langle lr \rangle_h$ will be high. Accordingly, the initially broad distribution of values of l (purple line) quickly relaxes to a much narrower distribution focused nearer the origin (red line), as shown in Fig. 4(b). This results in a rapid stress decay, giving negative $\dot{\sigma}$. Force balance demands the same negative $\dot{\sigma}$ in the solidlike region, in which $\langle lr \rangle_u$ is small. A stress decay (negative $\dot{\sigma}$) thus demands a negative $\dot{\gamma}_u$, i.e., a backwards elastic recoil of the solidlike region, as the material unloads. This elastic recoil advects the local strains of all elements in that solidlike region to lower values [Fig. 4(d)]—including into the negative range of l. Over a subsequent, slower timescale, these elements then plastically yield [Fig. 4(e)]. In particular, those elements that yield from negative l values and reset their l values to zero contribute a negative rate of stress relaxation $\langle lr \rangle_u$, giving a positive contribution to the stress rate of change, $\dot{\sigma} = \dot{\gamma}_u - \langle lr \rangle_u$. It is this plastic yielding of elements with negative l values that can give rise to the observed increase in the macroscopic stress. It does so for systems in which the shear bands prior to flow cessation had a sufficiently large
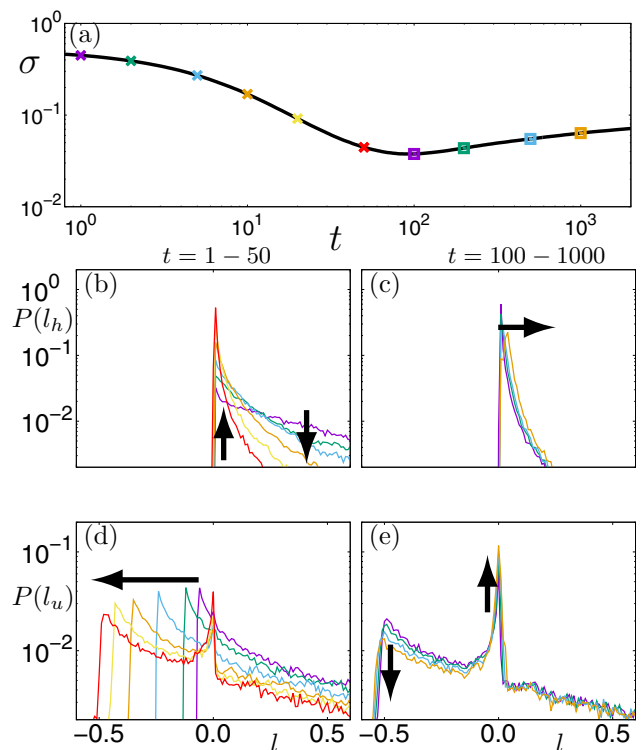

FIG. 4. Nonmonotonic stress decay as a function of time t after flow cessation. The distributions of local stresses are shown in panels (b) and (d) at times denoted by crosses during the initial stress decrease in (a). Panels (c) and (e) show the distributions during the later stress increase, at times denoted by squares in (a). Panels (b) and (c) pertain to the region previously (during flow) occupied by the high shear band. Panels (d) and (e) pertain to the region previously occupied by the low shear band. (b) In the liquidlike region, elements with positive values of l plastically yield at early times, causing the stress to relax. (c) At longer times in this region, the distribution shifts slightly to higher local strain values. (d) In the solidlike region, the distribution shifts elastically leftwards to lower local strain values during the initial stress relaxation. (e) At longer times in the solidlike region, elements with negative values of l plastically yield. It is this yielding of negative local stresses that results in the increase in macroscopic stress. Parameter values are $a = 6$, $\tau_x = 100$, $\bar{\dot{\gamma}} = 0.08$, and $\lambda = 0.005$. Arrows in (b)–(e) indicate increasing time.

difference in effective temperature, and in which the decay time for relaxation after flow cessation is sufficiently slow. This results in a separation of timescales between (first) the initially fast plastic yielding of positive local stresses from the fluidised band, which causes the initial rapid decay of the macroscopic stress; and (second) the later plastic yielding of negative local stresses from the solid band, which causes the slow rise in macroscopic stress.

Conclusions. We have shown that nonmonotonic stress relaxation after flow cessation can originate from an interplay between shear bands present prior to flow cessation. After flow cessation, a rapid plastic stress decay in the fluidized band couples via force balance to give an elastic recoil in the solidlike band. This causes the distribution of local stresses in the solid band to shift to include negative values. The subsequent plastic yielding of these negatively stressed elements,

on a longer timescale due to the lower effective temperature of this band, then contributes a slow increase to the macroscopic stress. These two distinct regimes in the stress evolution are strongly reminiscent of observations in boehmite gels [20] and self-associated organo/supramolecular gels [21]. We have considered throughout a nonzero noise temperature, for which the terminal time for stress relaxation is large but finite. It would be interesting in future work to consider model predictions at zero temperature, potentially allowing perma-

nent residual stresses, with their important implications for material performance.

Data availability. Our supporting research dataset is published in the Durham University research data repository [35].

[1] R. G. Larson, *The Structure and Rheology of Complex Fluids* (OUP, New York, 1999).

[2] L. Berthier and G. Biroli, Theoretical perspective on the glass transition and amorphous materials, Rev. Mod. Phys. **83**, 587 (2011).

[3] A. Nicolas, E. E. Ferrero, K. Martens, and J.-L. Barrat, Deformation and flow of amorphous solids: Insights from elastoplastic models, Rev. Mod. Phys. **90**, 045006 (2018).

[4] D. Bonn, M. M. Denn, L. Berthier, T. Divoux, and S. Manneville, Yield stress materials in soft condensed matter, Rev. Mod. Phys. **89**, 035005 (2017).

[5] T. Divoux, E. Agoritsas, S. Aime, C. Barentin, J.-L. Barrat, R. Benzi, L. Berthier, D. Bi, G. Biroli, D. Bonn *et al.*, Ductile-to-brittle transition and yielding in soft amorphous materials: perspectives and open questions, Soft Matter, **20**, 6868 (2024).

[6] M. Ballauff, J. M. Brader, S. U. Egelhaaf, M. Fuchs, J. Horbach, N. Koumakis, M. Krüger, M. Laurati, K. J. Mutch, G. Petekidis, M. Siebenbürger, T. Voigtmann, and J. Zausch, Residual stresses in glasses, Phys. Rev. Lett. **110**, 215701 (2013).

[7] E. Moghimi, A. R. Jacob, and G. Petekidis, Residual stresses in colloidal gels, Soft Matter **13**, 7824 (2017).

[8] L. Mohan, R. T. Bonnecaze, and M. Cloitre, Microscopic origin of internal stresses in jammed soft particle suspensions, Phys. Rev. Lett. **111**, 268301 (2013).

[9] V. V. Vasisht, P. Chaudhuri, and K. Martens, Residual stress in athermal soft disordered solids: insights from microscopic and mesoscale models, Soft Matter **18**, 6426 (2022).

[10] C. O. Osuji, C. Kim, and D. A. Weitz, Shear thickening and scaling of the elastic modulus in a fractal colloidal system with attractive interactions, Phys. Rev. E **77**, 060402(R) (2008).

[11] A. S. Negi and C. O. Osuji, Physical aging and relaxation of residual stresses in a colloidal glass following flow cessation, J. Rheology **54**, 943 (2010).

[12] S. Fritschi, M. Fuchs, and T. Voigtmann, Mode-coupling analysis of residual stresses in colloidal glasses, Soft Matter **10**, 4822 (2014).

[13] N. Pashine, D. Hexner, A. J. Liu, and S. R. Nagel, Directed aging, memory, and nature's greed, Sci. Adv. **5**, eaax4215 (2019).

[14] N. C. Keim and P. E. Arratia, Mechanical and microscopic properties of the reversible plastic regime in a 2D jammed material, Phys. Rev. Lett. **112**, 028302 (2014).

[15] S. Mukherji, N. Kandula, A. K. Sood, and R. Ganapathy, Strength of mechanical memories is maximal at the yield point of a soft glass, Phys. Rev. Lett. **122**, 158001 (2019).

[16] N. C. Keim, J. D. Paulsen, Z. Zeravcic, S. Sastry, and S. R. Nagel, Memory formation in matter, Rev. Mod. Phys. **91**, 035002 (2019).

[17] S. Hirobe, K. Imakita, H. Aizawa, Y. Kato, S. Urata, and K. Oguni, Simulation of catastrophic failure in a residual stress field, Phys. Rev. Lett. **127**, 064301 (2021).

[18] S. Kooij, G. van Dalen, J.-F. Molinari, and D. Bonn, Explosive fragmentation of prince rupert's drops leads to well-defined fragment sizes, Nat. Commun. **12**, 2521 (2021).

[19] P. Withers, Residual stress and its role in failure, Rep. Prog. Phys. **70**, 2211 (2007).

[20] I. Sudreau, M. Auxois, M. Servel, E. Lécolier, S. Manneville, and T. Divoux, Residual stresses and shear-induced overaging in boehmite gels, Phys. Rev. Mater. **6**, L042601 (2022).

[21] J. Hendricks, A. Louhichi, V. Metri, R. Fournier, N. Reddy, L. Bouteiller, M. Cloitre, C. Clasen, D. Vlassopoulos, and W. J. Briels, Nonmonotonic stress relaxation after cessation of steady shear flow in supramolecular assemblies, Phys. Rev. Lett. **123**, 218003 (2019).

[22] K. A. Murphy, J. W. Kruppe, and H. M. Jaeger, Memory in nonmonotonic stress relaxation of a granular system, Phys. Rev. Lett. **124**, 168002 (2020).

[23] Y. Lahini, O. Gottesman, A. Amir, and S. M. Rubinstein, Nonmonotonic aging and memory retention in disordered mechanical systems, Phys. Rev. Lett. **118**, 085501 (2017).

[24] R. Mandal, D. Tapias, and P. Sollich, Memory in nonmonotonic stress response of an athermal disordered solid, Phys. Rev. Res. **3**, 043153 (2021).

[25] Y. M. Joshi, Thixotropy, nonmonotonic stress relaxation, and the second law of thermodynamics, J. Rheology **66**, 111 (2022).

[26] R. Larson, Constitutive equations for thixotropic fluids, J. Rheology **59**, 595 (2015).

[27] J. Choi, M. Armstrong, and S. A. Rogers, The role of elasticity in thixotropy: Transient elastic stress during stepwise reduction in shear rate, Phys. Fluids **33**, 033112 (2021).

[28] D. Vlassopoulos, Personal communication (2024).

[29] P. Sollich, F. Lequeux, P. Hébraud, and M. E. Cates, Rheology of soft glassy materials, Phys. Rev. Lett. **78**, 2020 (1997).

[30] P. Sollich, Rheological constitutive equation for a model of soft glassy materials, Phys. Rev. E **58**, 738 (1998).

[31] J. P. Bouchaud, Weak ergodicity breaking and aging in disordered systems, J. Phys. I France **2**, 1705 (1992).

[32] S. M. Fielding, P. Sollich, and M. E. Cates, Aging and rheology in soft materials, J. Rheology **44**, 323 (2000).

[33] S. M. Fielding, M. E. Cates, and P. Sollich, Shear banding, aging and noise dynamics in soft glassy materials, Soft Matter **5**, 2378 (2009).

[34] G. Picard, A. Ajdari, F. Lequeux, and L. Bocquet, Elastic consequences of a single plastic event: A step towards the microscopic modeling of the flow of yield stress fluids, Eur. Phys. J. E **15**, 371 (2004).

[35] http://doi.org/10.15128/r1bz60cw31v.